Robust Predictive Battery Thermal Management Strategy for Connected and Automated Hybrid Electric Vehicles Based on Thermoelectric Parameter Uncertainty

Chong Zhu, *Member, IEEE*, Fei Lu, *Member, IEEE*, Hua Zhang, *Member, IEEE*, and Chunting Chris Mi, *Fellow, IEEE*

***Abstract*— The connected and automated hybrid electric vehicles (CAHEVs) have the potential to improve safety and mitigate traffic congestions. A crucial problem of the CAHEVs is that the lithium-ion batteries are highly temperature sensitive, whose output power is severely limited at low temperatures. Moreover, the cells may be premature aging at high operating temperatures and even result in an explosion, seriously threatening the human safety. Consequently, a practical and energy-efficient battery thermal management (BTM) strategy is required with the minimum possible cooling/heating energy consumption. To achieve the multiple objectives, a finite-set based model predictive control (FSMPC) strategy is presented for the BTM in CAHEVs. Since the thermoelectric model of the BTM system is highly nonlinear and time variant, an extended state observer is implemented for accurate system state estimation and prediction so that the parameter uncertainties inherent in the system can be compensated. The hardware-in-the-loop validation of the proposed strategy is conducted on the urban dynamometer drive schedule-based on a Toyota Prius plug-in HEV model. The results demonstrate that the proposed BTM strategy can maintain the battery pack in the CAHEV operating at the optimum temperature and save 30% BTM energy compared to the conventional method even under 50% parameter uncertainty.**

***Index Terms*— Battery thermal management (BTM), connected and automated hybrid electric vehicle (CAHEV), energy saving, extended state observer (ESO), model predictive control.**

I. Introduction

HYBRID electric vehicles (HEVs) are more energy efficient and cleaner than conventional vehicles [1], [2]. Recently, the connected and automated driving system has been applied to HEVs to further reduce fuel consumption along with the improvement of safety and traffic congestion [3]–[5]. The connected and automated HEVs (CAHEVs) include with advanced sensor technologies can provide real-time local information about current road conditions, which can be aggregated and analyzed to predict future road information and provide timely local feedback through intelligent transportation systems. Therefore, the optimized vehicle drive cycle can be achieved by the automated drive system in real time, leading to a considerable reduction of congestion, travel time, and fuel consumption [6].

However, CAHEVs involve several technical challenges, among which the battery thermal management (BTM) is crucial. For the commonly used lithium-ion batteries, low working temperatures such as −20 °C to −10 °C lead to slower chemical reactions, resulting in reduced power and available energy of the cell, as well as severe battery degradation [7]. Also, high working temperatures can reduce the lifetime and threaten the safety of the batteries, even cause permanent damage [8]. Therefore, the lithium-ion battery has to operate within a range of 15 °C–35 °C to ensure safety, optimum performance, and long service life [9].

Extensive research efforts have been made to focus on active BTM strategies with external air and liquid cooling/heating to improve both the system performance and efficiency. References [10]–[16] developed the detailed thermoelectric model of the BTM system in HEVs for better controllability, in which the heat generation mechanism, heat dissipation rate, and temperature uniformity are thoroughly discussed. Several global optimization methods, such as Pontryagin's maximum principle [17], dynamic programming [18]–[20], and nonlinear programming [21], have been performed on predefined road cycles to obtain reduced BTM energy consumption. However, the actual road cycles cannot well coincident with the preset fundamental road cycles because they are affected by randomized factors, e.g., weather conditions, traffic congestion, and driving styles. Consequently, the system performance and efficiency of these BTM strategies are degraded, because the merit of future road profile prediction in CAHEVs is not fully exploited. To enhance the applicability and real-time performance in CAHEVs, some online BTM strategies are also developed with the implementation of back stepping control [22], nonlinear model predictive control [23]–[25], and constrained linear quadratic predictive control [26], etc., in which accurate BTM models and associated parameters

Manuscript received January 7, 2018; revised April 5, 2018 and June 3, 2018; accepted June 19, 2018. Date of publication July 2, 2018; date of current version October 30, 2018. This work was supported by the U.S. Department of Energy under Grant DE-AR0000797. Recommended for publication by Associate Editor Marco Rivera (GE). *(Corresponding author: Chunting Chris Mi.)*

The authors are with the Department of Electrical and Computer Engineering, San Diego State University, San Diego, CA 92182 USA (e-mail: cmi@sdsu.edu).

Color versions of one or more of the figures in this paper are available online at http://ieeexplore.ieee.org.

Digital Object Identifier 10.1109/JESTPE.2018.2852218

are required. To deal with this issue, various methods are proposed for extracting the thermoelectric parameters of BTM systems [27]–[32].

Nevertheless, the performance and efficiency of the BTM system in CAHEVs are still challenged due to the complicated and nonlinear system model and parameters. Previous thermoelectric parameter estimation methods require offline experiments to provide look-up tables, for which a mass of preliminary work should be completed to deal with various BTM system configurations under different operating conditions, such as battery system-on-a-chip (SOC), air and liquid flow mass rates, and ambient temperature. Moreover, thermoelectric parameters of each BTM system in the same vehicle model present diversities because of the inherent parametric consistency of lithium-ion power batteries, such that the applicability and accuracy of the offline parameter test and measurement cannot be guaranteed. In order to enhance the system robustness against parameter uncertainties, the proportional—integral—differential (PID) controllers are still widely implemented in HEVs' BTM strategy regulate the air and liquid cooling/heating power separately [33]. Although this method can maintain the battery temperature to a reasonable range, the controllability of the consumed energy is unavailable due to the single-degree freedom of the PID controller, so that the energy optimization is hard to obtain.

In this paper, the BTM model is highly nonlinear and time variant, so that the analytical results of the optimization problem cannot be obtained through a closed-form equation. Instead, the numerical method has to be implemented to solve the minimum value problem of the cost function in the BTM system. Because the optimization method such as dynamic programming and nonlinear programming requires a large amount of computational resources, they are not practical for a long-term prediction in the real-time applications. To achieve the desired real-time performance, the finite-set-based predictive control method is proposed in this paper to discretize the control inputs to several combinations of the air and liquid mass flows. Then, the approximate minimum value of the cost function can be solved by the numerical method to obtain energy-efficient temperature control. In this method, the future road profile information of CAHEVs is entirely used to predict the battery temperature and evaluate the performances of possible solutions in the finite set. To avoid the preliminary measurements and enhancing the parameter robustness, a real-time estimation method based on an extended state observer (ESO) is proposed, which can precisely estimate the effect of the parameter uncertainties on the BTM system. With this method, proper compensation can be implemented to eliminate the influence of the parameter uncertainties. The hardware-in-the-loop (HIL) tests based on a 2010 Toyota Prius plug-in HEV (PHEV) model are implemented to validate the effectiveness and energy saving of the proposed robust predictive BTM strategy for CAHEVs.

II. Configuration and Mathematical Model of BTM System in CAHEVs

A. BTM System Configuration in HEVs

The air cooling/heating system uses several fans to drive the cabin air directly flowing past the surface of battery cells.

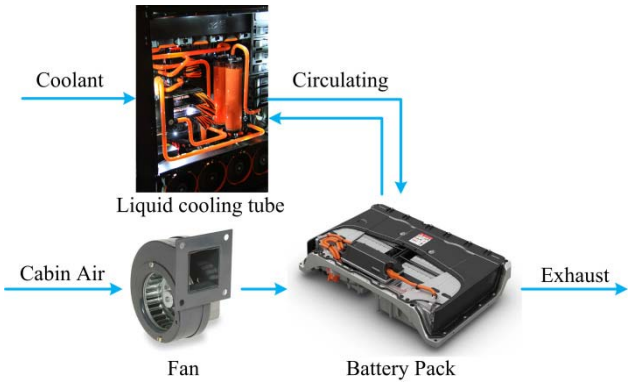

Fig. 1. Air and indirect liquid combined BTM system for HEVs.

The air-based BTM system is preferred by HEV manufacturers due to its simplicity and low cost. However, for large-scale battery cells discharging at high C-rates in plug-in HEVs, the liquid cooling/heating system is preferred for its better temperature regulation ability but with increased complexity, cost, and potential leakage problem. To fully use the merits of both systems, some HEV manufacturers combine the two systems in HEV models to obtain the optimum performance. In this paper, the air and liquid combined cooling/heating system is chosen as the BTM system configuration to achieve better efficiency, cost, and safety. The architecture of the BTM system is shown in Fig. 1.

B. Control-Oriented Model

As the BTM system is a nonlinear, time-variant system, its mathematical model cannot be directly implemented for control. Thus, a proper level of model simplification is required for the temperature control purpose. In this paper, a control-oriented thermoelectric model is developed for the implementation of model predictive BTM strategy.

As shown in Fig. 2(a), the battery electric behavior is described by an equivalent circuit containing a voltage source $V_{\rm oc}$ and an internal resistance $R_{\rm bat}$ [11]. Note that the battery parameters are influenced by the temperature and the SOC, as shown in Fig. 2(b) and (c). In addition, the battery aging can result in the battery parameter variation after several times of charging/discharging. The battery charge/discharge current can be expressed by

$$I_{\rm bat} = P_{\rm bat}/V_{\rm bat} \tag{1}$$

where $P_{\rm bat}$ is the battery power, and the terminal voltage $V_{\rm bat}$ can be represented as

$$V_{\rm bat} = V_{\rm oc} - R_{\rm bat} I_{\rm bat}. \tag{2}$$

Substituting (1) into (2), the battery charge/discharge current can be calculated as

$$I_{\rm bat} = \left(V_{\rm oc} - \sqrt{V_{\rm oc}^2 - 4P_{\rm bat}R_{\rm bat}}\right)/2R_{\rm bat} \tag{3}$$

where $P_{\rm bat}$ is the output power of the battery. Battery's SOC can be expressed as

$$\mathrm{SOC}^g = -I_{\rm bat}/C_{\rm bat} = \left(\sqrt{V_{\rm oc}^2 - 4P_{\rm bat}R_{\rm bat}} - V_{\rm oc}\right)/2R_{\rm bat}C_{\rm bat}. \tag{4}$$

The battery open-circuit voltage $V_{\rm oc}$ and internal resistance $R_{\rm bat}$ are affected by the temperature and SOC. However, they

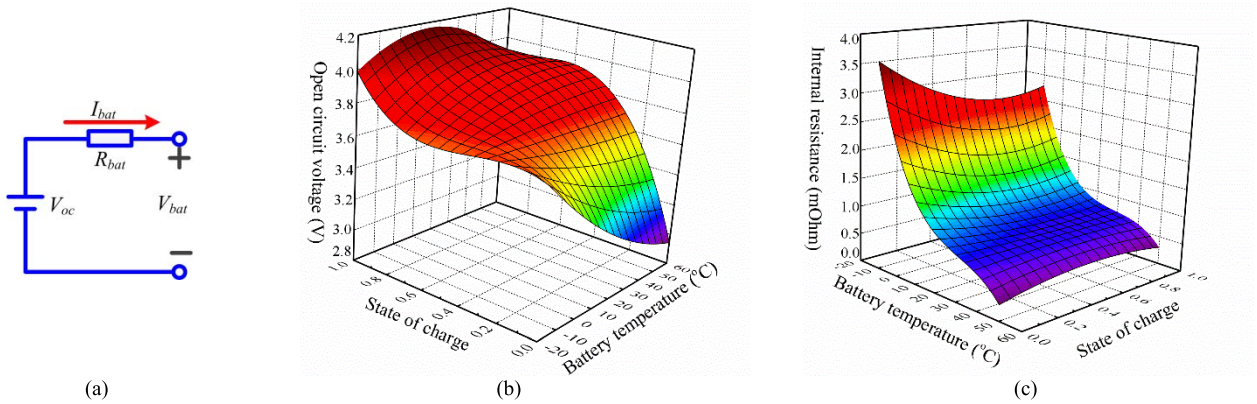

(a) (b) (c)

Fig. 2. Proposed battery electric model. (a) Equivalent circuit diagram of the battery pack. (b) Open-circuit voltage of battery cell. (c) Internal resistance of battery cell.

are assumed to be constant within a short period because of the slow dynamics of the battery temperature.

As for the controller design purpose, the uneven battery temperature distribution caused by the diffusion is not considered, because it is affected by the heat dissipation design and is complicated to model. Therefore, a lumped-parameter thermal model is chosen to effectively represent the dynamic changes of battery pack temperature, in which the battery cell is considered to have the same core and surface temperatures. According to the energy balancing principle, any change in battery temperature can be described as a heat balance around the module

$$\dot{T_{\text{bat}}} = (Q_{\text{gen}} + Q_{\text{exh}} - Q_{\text{air}} - Q_{\text{liq}})/C_{p,\text{bat}}m_{\text{bat}} \tag{5}$$

where Q_{gen} denotes the heat generation rate, Q_{air} and Q_{liq} are rates of the heat dispersed by air and liquid flows, respectively. Q_{exh} denotes the unknown heat source coupled by the powertrain, such as engine exhausted heat. The unit of Q_{gen}, Q_{air}, Q_{liq}, and Q_{exh} is J/s. $C_{p,\text{bat}}$ and m_{bat} stand for the module thermal capacity and mass, whose units are J/(kg · K) and kg, respectively.

The general energy balanced battery thermal model is developed in [10] for estimating the heat generation rate of the battery pack, which is expressed as

$$Q_{\text{gen}} = I_{\text{bat}}^2 R_{\text{bat}} - I_{\text{bat}} T_{\text{bat}} \frac{dV_{\text{oc}}}{dT_{\text{bat}}}. \tag{6}$$

The heat generation rate comprises two heat source terms: the irreversible Joule heat caused by the internal resistance (the first item) and the reversible entropy heat (the second item) caused by the entropy change during the chemical reactions in the battery. $dV_{\text{oc}}/dT_{\text{bat}}$ is a thermoelectric parameter only related to the type of the battery cell. Thus, the battery generates the entropy heat during the discharging ($I_{\text{bat}} > 0$) and absorbs the entropy heat during the charging ($I_{\text{bat}} < 0$). Meanwhile, the heat dissipation model can be established using the theory of uniform wall [34]; thus Q_{air} and Q_{liq} can be calculated by

$$Q_{\text{air}} = C_{p,\text{air}}m_{\text{air}}(T_{\text{bat}} - T_{\text{cab}})[1 - \exp(-h_{\text{air}}A_{\text{air}}/C_{p,\text{air}}m_{\text{air}})] \tag{7}$$

$$Q_{\text{liq}} = C_{p,\text{liq}}m_{\text{liq}}(T_{\text{bat}} - T_{\text{liq}})[1 - \exp(-h_{\text{liq}}A_{\text{liq}}/C_{p,\text{liq}}m_{\text{liq}})] \tag{8}$$

where $C_{p,\text{air}}$ and $C_{p,\text{liq}}$ denote the thermal capacity of the air and the coolant. T_{cab} and T_{liq} indicate the temperature of the cabin air and the coolant, respectively. m_{air} and m_{liq} denote the air and coolant flow mass rates, whose unit is kg/s. In this paper, T_{cab} is assumed to be constant for simplicity, as the air conditioner can regulate the cabin temperature within a small range. Reasonably, T_{liq} is also assumed to be constant, as the heat dissipated by the coolant can be totally exchanged in the heat pump. The corresponding heat transfer areas are denoted by A_{air} and A_{liq}. Meanwhile, the equivalent heat transfer coefficients are h_{air} and h_{liq}, whose unit is J/(m^2 · K). It should be noted that h_{air} and h_{liq} are time variant and have highly nonlinear characteristics, which are dependent on the temperature, battery, and the air and liquid mass flow rates.

The thermoelectric model of BTM system is described by (3)–(8), in which the air and liquid mass flow rates m_{air} and m_{liq} are considered as system inputs, and the battery temperature and SOC are system states. The consumed electric power of air and liquid cooling/heating can be regarded as approximately proportional to the cubic of the system inputs m_{air} and m_{liq}, e.g., $P_{\text{air}} = K_{\text{air}}m_{\text{air}}^3$ and $P_{\text{liq}} = K_{\text{liq}}m_{\text{liq}}^3$. The air and liquid mass flow rates should be well controlled to obtain the optimum temperature T_{bat} with the minimum possible consumed energy. The thermoelectric parameters in (3)–(8), such as V_{bat}, R_{bat}, h_{air}, and h_{liq}, are usually obtained by preliminary offline experiments and measurements, which are time consuming and less accurate due to the inherent battery parameter inconsistency. For better performance and efficiency, an online estimation method will be introduced in Section IV to compensate the parameter uncertainties.

III. Finite-Set Based Model Predictive BTM Strategy for CAHEVs

As the thermoelectric battery model is highly nonlinear and time variant, the controllers used in the linear system are not applicable. Therefore, the finite-set-based model predictive control is implemented to regulate the battery temperature for its robustness and simplicity. The future driving profile in CAHEVs can be used to predict the potential battery power. Thus, the battery temperature in accordance with thermal management power can be predicted to evaluate the thermal management effect and associated energy consumption.

A. Battery Temperature Prediction

According to the thermoelectric battery model presented by (5), the control-oriented discrete prediction function for the battery temperature in CAHEVs can be built

$$\begin{aligned} T_{\text{bat}}(k+i) = {} & T_{\text{bat}}(k+i-1) + T_s \\ & \times [Q_{\text{gen}}(k+i-1) - Q_{\text{air}}(k+i-1) \\ & - Q_{\text{liq}}(k+i-1)]/C_{p,\text{bat}} m_{\text{bat}} \end{aligned} \tag{9}$$

where T_s is the sampling period, and $i = 0, 1, 2, \ldots, H$. H is the prediction horizon. The heat dissipation rates Q_{air} and Q_{liq} are discretized as

$$\begin{aligned} Q_{\text{air}}(k+i) = {} & C_{p,\text{air}} m_{\text{air}}(k+i)[T_{\text{bat}}(k+i) - T_{\text{cab}}(k+i)] \\ & \{1 - \exp[-h_{\text{air}} A_{\text{air}}/C_{p,\text{air}} m_{\text{air}}(k+i)]\} \end{aligned} \tag{10}$$

$$\begin{aligned} Q_{\text{liq}}(k+i) = {} & C_{p,\text{liq}} m_{\text{liq}}(k+i)[T_{\text{bat}}(k+i) - T_{\text{liq}}(k+i)] \\ & \{1 - \exp[-h_{\text{liq}} A_{\text{liq}}/C_{p,\text{liq}} m_{\text{liq}}(k+i)]\} \end{aligned} \tag{11}$$

The battery temperature and consumed cooling/heating power during the prediction horizon are available by using the proposed prediction functions (9)–(11). For CAHEVs, there is an outstanding feature that the future drive information during the prediction horizon can be obtained from the intelligent electronic control unit (ECU) in advance. Therefore, the future propulsion power of the vehicle can be used to predict the potential charge/discharge power P_{bat}, then $Q_{\text{gen}}(k)$ can be predicted by the proposed thermoelectric model. Consequently, a long prediction horizon for the BTM system in CAHEVs, e.g., 30 s or even 1 min, can be implemented to significantly improve the system efficiency.

The remaining SOC is selected to evaluate the BTM system efficiency, which is expressed as

$$\begin{aligned} & \text{SOC}(k+i) \\ & = \text{SOC}(k+i-1) - T_s/2C_{\text{bat}} R_{\text{bat}} \\ & \quad \cdot \left[V_{\text{oc}}(k+i-1) - \sqrt{V_{\text{oc}}^2(k+i-1) - 4P_{\text{bat}}(k+i-1) R_{\text{bat}}} \right]. \end{aligned} \tag{12}$$

In (12), the BTM power $P_{\text{air}}(k)$ and $P_{\text{liq}}(k)$ should be also contained in $P_{\text{bat}}(k)$ to evaluate the BTM system efficiency.

B. Cost Function Selection

In order to obtain the optimum battery temperature with the minimum required energy cost, a cost function should be used to evaluate the performances of the possible solutions in the finite set. Since the battery temperature and the energy saving are both the control targets, they should be both considered in the cost function.

It is known that the critical high or low temperatures can accelerate the aging of the battery cells, resulting in premature of the battery packs. Meanwhile, under the low temperatures, the battery capacity is severely deteriorated, leading to the limited output power. Therefore, the cost function should provide a relatively high punishment against low temperatures compared with the optimum working temperatures. Moreover, a very high temperature may result in the thermal failure of the batteries, even leading to explosion. Thus, the critical high temperatures should take much more punishment than the critical low temperatures in the cost function, representing that the BTM system should pay more attention to the critical high temperatures to ensure safety. To meet both requirements, Lopez-Sanz *et al.* [23], [24] proposed a temperature punishment function based on the battery type, aging performance, and electric parameters under different temperatures, which is implemented in this paper

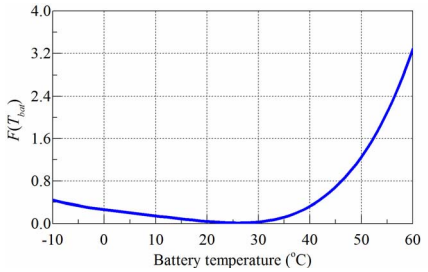

Fig. 3. Battery temperature punishment function.

$$F(k) = \alpha_0 - \alpha_1 T_{\text{bat}}(k) + \alpha_2 T_{\text{bat}}^2(k) - \alpha_3 T_{\text{bat}}^3(k) + \alpha_4 T_{\text{bat}}^4(k) \tag{13}$$

where $\alpha_0 = 0.2636, \alpha_1 = 1.285\text{e-}2, \alpha_2 = 2.47\text{e-}4, \alpha_3 = 1.847\text{e-}5$, and $\alpha_4 = 5.316\text{e-}7$, which are corresponding coefficients obtained through curve fitting. The punishment curve against battery temperature is shown in Fig. 3. It is obvious that the cost function provides very high punishment values at critical high temperature to ensure the safe operation and the less aging effect. The critically low battery temperatures are also punished by relatively high values for better aging performance and more available output power. The optimum operating temperature range between 20 °C and 35 °C is acceptable according to the manufacturer, which is also represented in the cost function curve.

As to the energy consumption, a straightforward evaluation approach is to calculate the consumed SOC. Consequently, the cost function for the FSMPC is established as

$$J(k) = \mu F(k+H) + (1-\mu)[1 - \text{SOC}(k+H)] \tag{14}$$

where $\mu \in (0, 1)$ is the coefficient to tune the weighting factor between the BTM system performance and efficiency. From (14), it is concluded that the proposed cost function can efficiently evaluate both the battery temperature and the energy cost, which applies to the proposed FSMPC method for BTM system in CAHEVs.

C. Finite-Set-Based MPC BTM Strategy

Since the BTM model described by (3)–(8) is a highly nonlinear system, it is not possible to directly solve the optimum air and liquid cooling/heating powers. Thus, a finite-set based control strategy is proposed in this paper, in which the complicated resolving process can be avoided. Each solution is substituted in the long-horizon prediction model (9)–(11) to predict the battery temperature and SOC at the destination. Then, the cost function (14) is used to evaluate the related

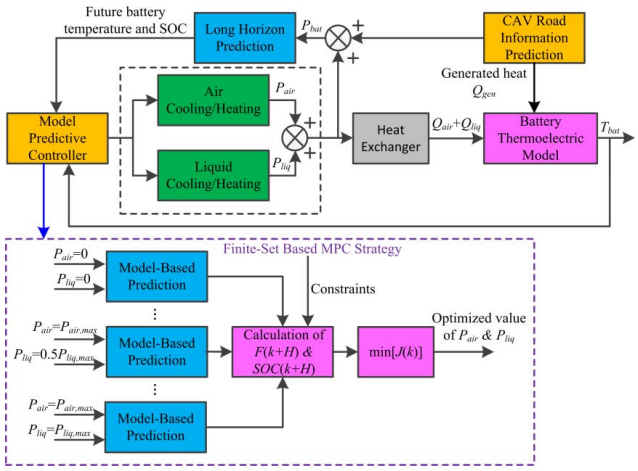

Fig. 4. Proposed FSMPC scheme for BTM system in CAHEVs.

performances of these possible solutions, in which the optimized combination of the cooling/heating powers is selected for improving both the battery temperature and energy saving

$$[P_{\text{air,opt}}(k), P_{\text{liq,opt}}(k)] = \underset{[P_{\text{air}}(k), P_{\text{liq}}(k)] \in P}{\text{minimize}} J[k, P_{\text{air,opt}}(k), P_{\text{liq,opt}}(k)] \quad (15)$$

where the finite set of air and liquid cooling/heating system powers is expressed as $\{[\lambda_{\text{air}} P_{\text{air,max}}, \lambda_{\text{liq}} P_{\text{liq,max}}]\}$ ($\lambda_{\text{air}} = 0, 0.1, 0.2, \ldots, 1$, and $\lambda_{\text{liq}} = 0, 0.1, 0.2, \ldots, 1$). To balance the solving precision and the computational efforts, the number of possible solutions in the finite set is chosen as 100 in this paper. The control structure of the proposed finite-set model-based BTM prediction control is shown in Fig. 4. Due to the large time constant, the battery temperature changes slowly during a long prediction horizon. Therefore, the constant cooling/heating powers $P_{\text{air}}(k)$ and $P_{\text{liq}}(k)$ are assumed within the prediction horizon. This reasonable assumption can reduce the iteration times in each control period, leading to further alleviation of the ECU's computational burden for BTM systems.

IV. Parameter Uncertainty Compensation Based on ESO

A. Effect of Parameter Uncertainties on BTM System

As described above, the thermoelectric parameters are time variant and hard to measure directly in a BTM system. Thus, there is nonnegligible prediction error in both battery temperature and consumed energy predictions. Based on (9), the predicted battery temperature with overrated internal battery resistance is higher than its actual value; thus, more cooling power is required for the unsatisfactory battery temperature, leading to the decreased system efficiency. There is the same problem when the heat transfer coefficients h_{air} and h_{liq} are underestimated. Contrarily, if the heat generation source parameters are underestimated or the heat transfer coefficients are overrated, the cooling/heating of battery packs is insufficient. Moreover, the heat Q_{exh} coupled with the powertrain cannot be modeled with mathematical equations, producing an unpredictable influence on the battery temperature.

B. ESO-Based Parameter Uncertainty Compensation

The ESO is developed for active disturbance rejection control [35], which is verified to be effective in canceling the influence of parameter uncertainties. In a BTM system, the inherent system parameter uncertainties have an undesirable effect on system performance, which can be expressed as

$$\begin{aligned}\dot{T_{\text{bat}}} &= (Q_{\text{gen}} + Q_{\text{exh}} - Q_{\text{air}} - Q_{\text{liq}})/C_{p,\text{bat}} m_{\text{bat}} \\ &\quad + f(\Delta h_{\text{air}}, \Delta h_{\text{liq}}) \\ &= (-Q_{\text{air}} - Q_{\text{liq}})/C_{p,\text{bat}} m_{\text{bat}} + d \end{aligned} \quad (16)$$

where Δh_{air} and Δh_{liq} represent the offsets between the actual values and the estimated values of h_{air} and h_{liq}, respectively. Accordingly, $f(\Delta h_{\text{air}}, \Delta h_{\text{liq}})$ denotes the effect of the thermoelectric parameter variation of h_{air} and h_{liq}. Since the calculation of heat generation rate Q_{gen} requires precise battery parameters which are hard to obtain, it can also be considered as one of the system disturbances. Meanwhile, the unknown exhausted heat Q_{exh} can also be taken as the system disturbances. Thus, the total system disturbance d caused by system parameter uncertainties contains both the heat generation rate $(Q_{\text{gen}} + Q_{\text{exh}})$ and the effect of thermoelectric parameter mismatch.

To compensate the influence of parameter uncertainties, d is chosen as an extended system state in addition to T_{bat}. The state of the extended system is presented as

$$\begin{cases} \dot{x} = Ax + Bu + Eh \\ y = Cx \end{cases} \quad (17)$$

where $x = [T_{\text{bat}} d]^T$, $u = [Q_{\text{air}} Q_{\text{liq}}]^T$, $A = [00; 01]$; $B = -1/(C_{p,\text{bat}} m_{\text{bat}})[11; 00]$; $C = [10]$, $E = [01]^T$, and h represents the variation rate of the augment system state d. Based on (14), an ESO can be built as

$$\begin{cases} \dot{z} = Az + Bu + L\left(y - \hat{y}\right) \\ \hat{y} = Cz \end{cases} \quad (18)$$

where $z = [\hat{T}_{\text{bat}} \ \hat{d}]^T$ with the observer gain $L = [\beta_1 \ \beta_2]^T$. From the built ESO, the effect of the system parameter uncertainty d can be observed with the use of the difference between the measured battery temperature T_{bat} and the estimated battery temperature $\hat{T}_{\text{bat}}$. By transforming (18) into the discrete domain, the discrete ESO used in the BTM system is constructed as

$$\begin{cases} \hat{T}_{\text{bat}}(k+1) = \hat{T}_{\text{bat}}(k) + T_s \hat{d}(k) + \beta_1 T_s [T_{\text{bat}}(k) - \hat{T}_{\text{bat}}(k)] \\ \quad -T_s [Q_{\text{air}}(k) + Q_{\text{liq}}(k)]/C_{p,\text{bat}} m_{\text{bat}} \\ \hat{d}(k+1) = \hat{d}(k) + \beta_2 T_s [T_{\text{bat}}(k) - \hat{T}_{\text{bat}}(k)]. \end{cases} \quad (19)$$

Usually, the observer gains are selected as $\beta_1 = 2\ \omega_0$ and $\beta_1 = \omega_0^2$ to ensure both the system stability and the fast dynamics [36]. When considering the limitation of discrete sampling, the system bandwidth ω_0 is chosen as $\pi/3T_s$ to obtain both sufficient stability margin and fast dynamic response.

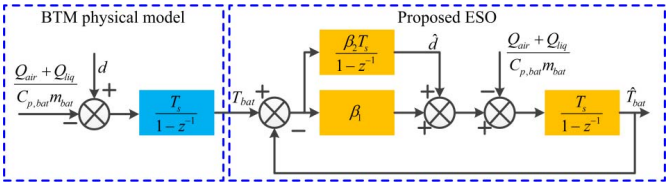

Fig. 5. Control diagram of the proposed ESO.

C. Parameter Uncertainty Compensation Analysis

Performing the Z transform on (18), the control diagram of the proposed ESO can be established to analyze the ability of parameter uncertainty compensation. As shown in Fig. 5, the observed battery temperature with the feedback of the actual battery temperature can be expressed as

$$\frac{\hat{T}_{\mathrm{bat}}(z)}{T_{\mathrm{bat}}(z)} = \frac{2\omega_0 T_s(1-z^{-1}) + \omega_0^2 T_s^2}{(1+\omega_0 T - z^{-1})^2}. \tag{20}$$

Then, the transfer function of disturbance estimation is expressed as

$$\frac{\hat{d}(z)}{d(z)} = \frac{\omega_0^2 T_s^2}{(1+\omega_0 T_s - z^{-1})^2}. \tag{21}$$

From (20) and (21), the transfer functions show that the proposed ESO is a second-order inertia plant, whose zeros and poles are determined by the observer gain β_1 and β_2. As the battery temperature changes slowly during the prediction horizon, its dynamics can be tracked by the fast second-order plant without steady errors. Consequently, the system disturbance d can also be precisely estimated as shown in (19), because it is observed according to the tracking error between $\hat{T}_{\mathrm{bat}}$ and T_{bat}. Consequently, the parameter uncertainties can be adequately compensated with the implementation of the proposed ESO.

D. Battery Temperature Prediction Based on ESO

As the proposed ESO can accurately estimate the system disturbances caused by heat generation Q_{gen} and parameter uncertainties $f(\Delta h_{\mathrm{air}}, \Delta h_{\mathrm{liq}})$, the battery temperature prediction function can be rewritten as

$$\begin{aligned} &T_{\mathrm{bat}}(k+i) \\ &= T_{\mathrm{bat}}(k+i-1) - T_s/C_{p,\mathrm{bat}}m_{\mathrm{bat}} \\ &\quad \times [Q_{\mathrm{air}}(k+i-1) + Q_{\mathrm{liq}}(k+i-1)] + T_s d(k+i-1). \end{aligned} \tag{22}$$

However, the future values of d used in the long horizon prediction still cannot be directly obtained from the ESO. To fix this issue, the numerical relation between future battery power and system disturbances is required. According to (3) and (6), the battery heat generation rate can be expressed as

$$\begin{aligned} Q_{\mathrm{gen}} = &\left(\frac{V_{\mathrm{oc}} - \sqrt{V_{\mathrm{oc}}^2 - 4P_{\mathrm{bat}}R_{\mathrm{bat}}}}{2R_{\mathrm{bat}}}\right)^2 R_{\mathrm{bat}} \\ &- \frac{T_{\mathrm{bat}}\left(V_{\mathrm{oc}} - \sqrt{V_{\mathrm{oc}}^2 - 4P_{\mathrm{bat}}R_{\mathrm{bat}}}\right)}{2R_{\mathrm{bat}}} \cdot \frac{dV_{\mathrm{oc}}}{dT_{\mathrm{bat}}}. \end{aligned} \tag{23}$$

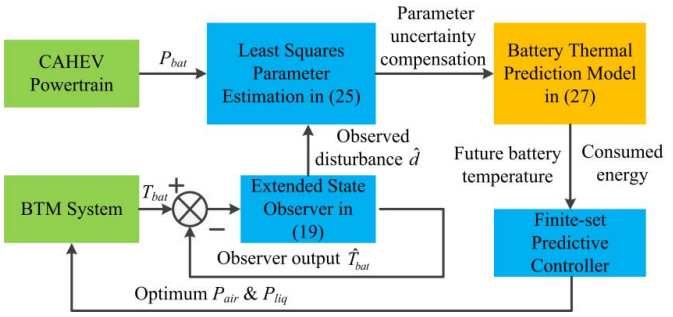

Fig. 6. Compensation of parameter uncertainties based on ESO.

Substituting (23) into (16) and performing the Taylor series expansion, the system disturbance can be approximately expressed as

$$\begin{aligned} d \doteq &\frac{R_{\mathrm{bat}}}{V_{\mathrm{oc}}^2}\left(1 - \frac{2R_{\mathrm{bat}}}{V_{\mathrm{oc}}^2}\right)P_{\mathrm{bat}}^2 + \frac{2R_{\mathrm{bat}}T_{\mathrm{bat}}}{V_{\mathrm{oc}}^2} \cdot \frac{dV_{\mathrm{oc}}}{dT_{\mathrm{bat}}} \cdot P_{\mathrm{bat}} \\ &+ f(\Delta h_{\mathrm{air}}, \Delta h_{\mathrm{liq}}) + Q_{\mathrm{exh}} - T_{\mathrm{bat}}\frac{dV_{\mathrm{oc}}}{dT_{\mathrm{bat}}} \\ \doteq &AP_{\mathrm{bat}}^2 + BP_{\mathrm{bat}} + C. \end{aligned} \tag{24}$$

As the coefficients in (24) are almost constant within the prediction horizon, the polynomial approximation can be made to simplify the control strategy, where three constant factors A, B, and C are used to describe the numerical relation between d and P_{bat}. Using the stored historical data of P_{bat} and d, the optimum values of A, B, and C can be estimated by the least-squares method

$$\begin{bmatrix} A \\ B \\ C \end{bmatrix} = (P^T P)^{-1} P^T \begin{bmatrix} d(k) \\ d(k-1) \\ \vdots \\ d(k-N) \end{bmatrix} \tag{25}$$

in which

$$P = \begin{bmatrix} 1 & P_{\mathrm{bat}}(k) & P_{\mathrm{bat}}^2(k) \\ 1 & P_{\mathrm{bat}}(k-1) & P_{\mathrm{bat}}^2(k-1) \\ \vdots & \vdots & \vdots \\ 1 & P_{\mathrm{bat}}(k-N) & P_{\mathrm{bat}}^2(k-N) \end{bmatrix} \tag{26}$$

where N denotes the number of the stored sampling data groups for the system parameter estimation. By combining (22)–(26), the future battery temperature can be predicted as

$$\begin{aligned} T_{\mathrm{bat}}(k+i) = &T_{\mathrm{bat}}(k+i-1) - T_s[Q_{\mathrm{air}}(k+i-1) \\ &+ Q_{\mathrm{liq}}(k+i-1)]/C_{p,\mathrm{bat}}m_{\mathrm{bat}} \\ &+ T_s\left[AP_{\mathrm{bat}}^2(k+i-1) + BP_{\mathrm{bat}}^2(k+i-1) + C\right]. \end{aligned} \tag{27}$$

In (27), the thermoelectric parameters of the BTM system are not required for battery temperature prediction, while the accuracy of this prediction can be guaranteed by the implementation of the ESO and the measurement of the battery temperature, as shown in Fig. 6. Therefore, the effect of parameter uncertainties can be eliminated, leading to the

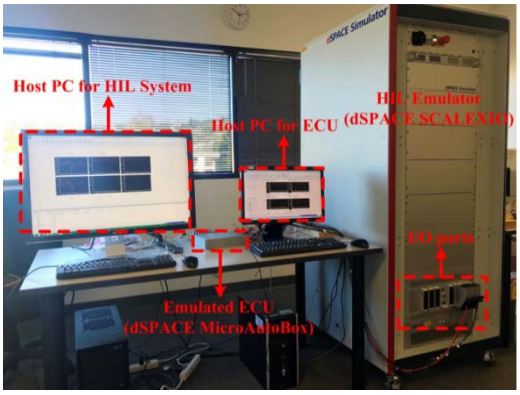

Fig. 7. Experimental setup of HIL test bench.

precise prediction of battery temperature and improved BTM system performance and efficiency.

V. Hardware-in-the-Loop Validation Results

A. HIL Test Configuration

The HIL test bench for the BTM system is shown in Fig. 7. The dSPACE MicroAutoBox is utilized for emulating the ECU in CAHEVs, in which the real-time optimized BTM strategy is implemented and tested. The HEV is emulated by the dSPACE SCALEXIO, in which the physical model of the BTM system is emulated as the control object in a real time. Note that the battery power is assumed to be precisely predicted by the intelligent transportation systems for CAHEVs during the drive cycle to avoid the influence of the stochastic process, such as immediate load change caused by the unpredictable traffic accidents.

The urban dynamometer driving schedule is implemented as the test drive cycle, and the Toyota Prius 2010 PHEV model is selected as the test vehicle model. The vehicle model is from Autonomie Rev. 15 SP1, containing the models of electric components, powertrain, engine, road conditions, and so on. The related vehicle parameters in the HIL test are provided by the technical test report of Idaho National Laboratory [36]. As the aging performance of the battery is not modeled in the test, the battery parameter uncertainties are set in the controller to represent the parameter inaccuracy caused by the battery aging. The exhausted heat Q_{exh} coupled by the powertrain is modeled as an unknown constant in the HIL test. The control period is set to 1 s, and the prediction horizon is set to 30 s to take full advantage of the CAHEV's future drive profiles in prediction. The full powers of the air and liquid cooling/heating systems are 150 and 700 W, respectively. The temperatures of the cabin air and the coolant are both set to 25 °C. The start points of the battery temperatures for cooling and heating tests are 50 °C and 0 °C, respectively.

B. HIL Test Results of the Weighting Factor μ

In order to study the influence of the weighting factor in the cost function on system performance, the HIL tests with different values of $\mu(0.1, 0.5, and 0.9)$ are conducted, and the results are shown in Fig. 8. It is clear that the battery temperature cannot reach to the optimal value (27 °C) when a small weighting factor ($\mu = 0.1$) is adopted. Contrarily, a large weighting factor ($\mu = 0.9$) leads to better temperature performance, but with much more BTM consumed energy, which is not preferable for energy saving. In order to balance the battery temperature performance and energy efficiency, the weighting factor is set to 0.5 in the HIL test.

C. HIL Test Results of the Proposed Strategy and Conventional Strategy

To verify the energy-efficiency of the proposed FSMPC BTM strategy, the HIL tests are performed. The weighing coefficient μ in the cost function is chosen as 0.5 to obtain both the desired battery temperature and the improved energy efficiency. The commonly used PID-based method is also tested to provide the comparison, in which the air-based and liquid-based systems are controlled by two PID regulators separately. The desired battery pack temperature in PID method is set to 27 °C according to its aging curve and output power limit.

The cooling performance of the BTM system is first presented in Fig. 9. As depicted in Fig. 9(b), the battery temperatures performances under the two tested methods are very similar, whose dynamics and final states are close to each other. Because the total consumed BTM system energy, namely, $W_{\text{air}} + W_{\text{liq}}$ shown in Fig. 9(c), is almost 30% off, the energy efficiency of the FCMPC-based system is obviously improved without deteriorating the control performance of the battery temperature. The resulted difference in system energy efficiency is due to different combinations of air-based and liquid-based system powers in the two methods, as shown in Fig. 9(a). To reduce the BTM energy consumption, the PID method tends to use more air-based system power under the assumption that the air-based system power is lower than the liquid-based system power. However, when the battery temperature is close to the cabin air temperature, the dissipated heat rate of the air-based system is significantly low even at the full power. This undesirable phenomenon is caused by the relatively low heat transfer coefficient h_{air} and thermal capacity $C_{p,\text{air}}$. Contrarily, the liquid-based system provides a higher energy efficiency when the temperatures of the coolant and the battery pack are close, because of h_{liq} and $C_{p,\text{liq}}$ are much higher than h_{air} and $C_{p,\text{air}}$.

Therefore, when the battery temperature is close to that of the cooling media, the liquid-based system can provide higher heat dissipation rate with a lower energy consumption, as shown in Fig. 9(c). To present the energy efficiency of the BTM system, the evaluation index is defined as $(Q_{\text{air}} + Q_{\text{liq}})/(P_{\text{air}} + P_{\text{liq}})$, as shown in Fig. 9(c). It can be seen that the proposed FSMPC BTM strategy can optimize the cooling power distribution to the air-based and liquid-based systems due to the evaluation of the cost function (14). Another merit of the proposed FSMPC is that the future battery temperature can be predicte; thus, the FSMPC-based BTM system possesses better capability to respond to foreseen vehicle driving profiles, leading to further BTM energy reduction.

The heating performance of the BTM system is also tested, and the results are shown in Fig. 10. Similar to the cooling

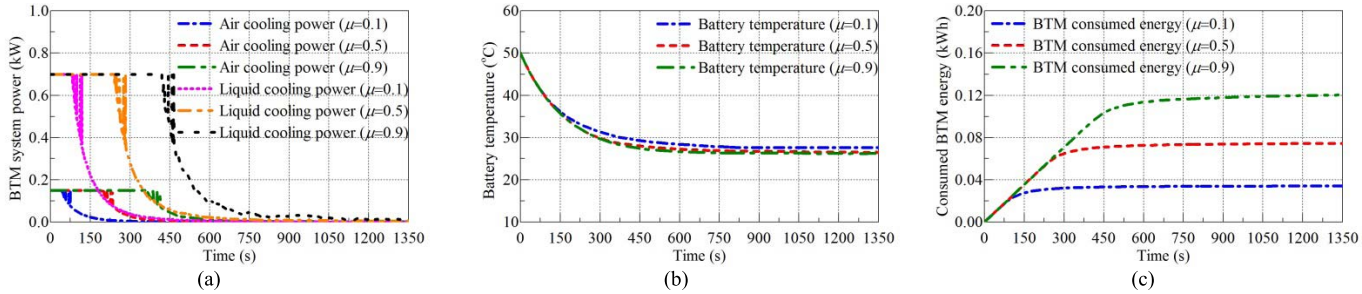

Fig. 8. HIL test results of BTM system performance with different weighting factors. (a) BTM system power. (b) Battery temperature. (c) Total consumed BTM energy.

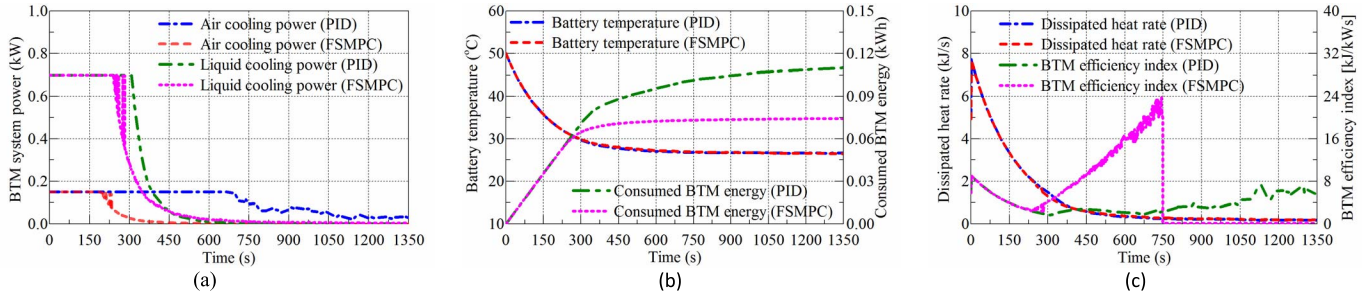

Fig. 9. HIL test results of BTM system's cooling performance. (a) BTM system power. (b) Battery temperature and consumed BTM energy. (c) Heat dissipation rate and energy-efficiency index of BTM system.

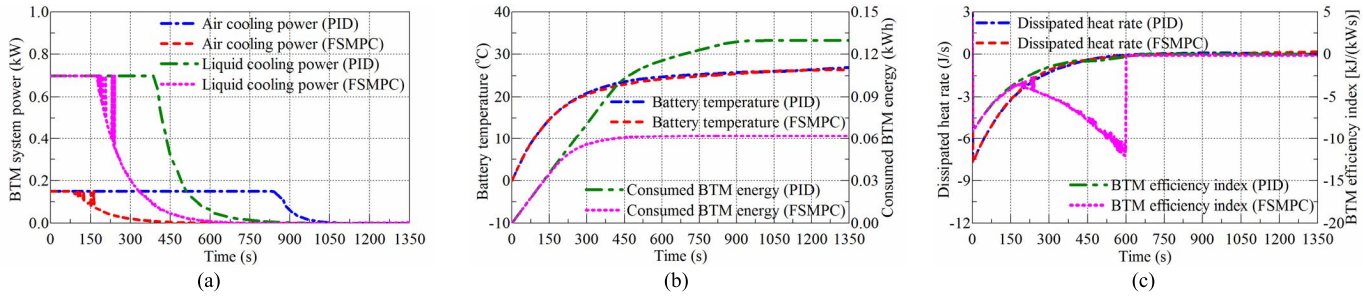

Fig. 10. HIL test results of BTM system's heating performance. (a) BTM system power. (b) Battery temperature and consumed BTM energy. (c) Heat dissipation rate and energy-efficiency index of BTM system.

performance, the proposed FSMPC strategy can save more than 50% energy compared to the conventional PID method with almost identical battery temperature control performance. It can be seen that both the air-based and liquid-based systems are OFF when the battery temperature reaches to 25 °C, because the cabin air and coolant cannot transfer heat to the battery anymore. The battery temperature can still rise due to the Joule heat generation. The HIL test results demonstrate that the proposed FSMPC can effectively cool/heat the battery pack to the optimum temperature during drive cycles with improved system energy efficiency.

D. HIL Test Results of the Parameter Uncertainty Compensation

The primary concern for the parameter variations is that the heat transfer coefficients h_{air} and h_{liq} are deteriorated by parametric uncertainties. Meanwhile, the battery internal resistance is also affected by the aging. Thus, the values of h_{air}, h_{liq}, and R_{int} are set with various deviations in the HIL test. In the test, 150% (120%) estimated h_{air} and h_{liq} are combined with 50% (80%) estimated R_{int}, leading to the predicted battery temperature lower than the actual value, as shown in Fig. 11(a). On the contrary, 50% (80%) estimated h_{air} and h_{liq} are combined with 150% (120%) estimated R_{int} in the test, resulting in the predicted battery temperature higher than the actual value, as shown in Fig. 11(b). Consequently, the HIL test results show the battery temperature cannot be cooled down to the optimum value when the predicted temperature is underestimated (150% estimated h_{air} and h_{liq} with 50% estimated R_{int}). Contrarily, the consumed BTM energy is increased dramatically when the predicted temperature is overrated (50% estimated h_{air} and h_{liq} with 150% estimated R_{int}), as shown in Fig. 11(c). It can be concluded that the uncompensated system cannot provide desired battery temperature performance and energy efficiency.

The proposed ESO-based FSMPC method is tested to validate its robustness against parameter uncertainties. As seen

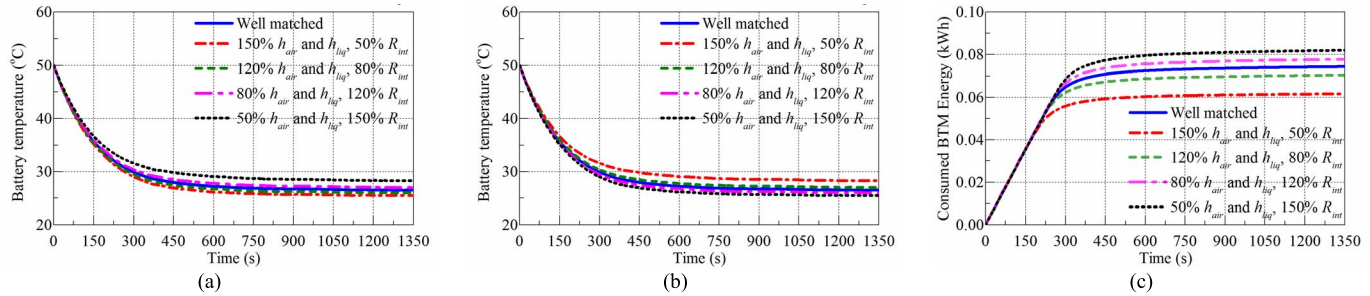

Fig. 11. HIL test results of BTM system performance with parameter mismatch. (a) Predicted battery temperature. (b) Actual battery temperature. (c) Total consumed BTM energy.

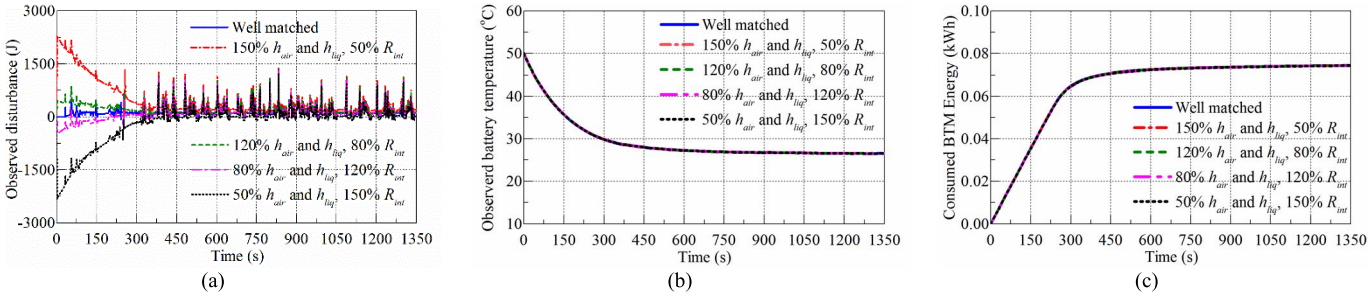

Fig. 12. HIL test results of the proposed ESO-based FCMPC BTM strategy with thermoelectric parameter mismatch. (a) Observed disturbances. (b) Battery temperature. (c) BTM consumed energy.

from Fig. 12(a), the disturbances caused by the parameter variations and model uncertainties are observed by the ESO. The convergence time of the observed system disturbance d is affected by the severity of system parameter uncertainties. Meanwhile, under the effect of the parameter mismatch, the tracked system disturbances deviate from the one without parameter uncertainties. These differences denote the influences of the parameter mismatch, which are precisely observed to provide a proper compensation in the battery temperature control, as shown in Fig. 12(b). Compared to the test results without the compensation, the influences of parameter uncertainties on consumed BTM energies are also eliminated, as shown in Fig. 12(c). The minor differences of the consumed energies are produced in the initial convergence of the system disturbance observation. The HIL test results show that the proposed FSMPC BTM strategy has strong robustness against parameter uncertainties so that the BTM system performance and efficiency can be both guaranteed at various operating scenarios.

VI. Conclusion

This paper has given a sufficient insight into the BTM in CAHEVs. To improve the system performance and energy efficiency, a finite-set model predictive BTM strategy is proposed to take advantage of both air-and liquid-based cooling/heating systems. By using CAHEVs' future driving profiles, the optimal combination of air and liquid cooling/heating power is achieved for regulating the battery temperature with the minimum possible electric energy. To eliminate the influence of the thermoelectric parameter variations and model uncertainties, the ESO is proposed. Then, the proper compensation based on the observed system disturbances can be achieved; thus the accuracy of the prediction model is significantly improved, leading to excellent parameter robustness. The HIL validation of the proposed BTM strategy is implemented on a Toyota Prius PHEV model. Compared to the conventional BTM method, the proposed FSMPC BTM strategy can save more than 30% electric energy of BTM system during the whole drive cycle without battery temperature performance deterioration. Meanwhile, the HIL validation results also show that the system performance and energy efficiency are immune to parameter uncertainties. In the future work, the stochastic load change during the drive cycle will be investigated to further enhance the robustness of the BTM system.

References

[1] D. W. Gao, C. Mi, and A. Emadi, "Modeling and simulation of electric and hybrid vehicles," *Proc. IEEE*, vol. 95, no. 4, pp. 729–745, Apr. 2007.

[2] N. Al-Aawar and A.-R. A. Arkadan, "Optimal control strategy for hybrid electric vehicle powertrain," *IEEE J. Emerg. Sel. Topics Power Electron.*, vol. 3, no. 2, pp. 362–370, Jun. 2015.

[3] D. Bevly *et al.*, "Lane change and merge maneuvers for connected and automated vehicles: A survey," *IEEE Trans. Intell. Vehicles*, vol. 1, no. 1, pp. 105–120, Mar. 2016.

[4] J. Rios-Torres and A. A. Malikopoulos, "A survey on the coordination of connected and automated vehicles at intersections and merging at highway on-ramps," *IEEE Trans. Intell. Transp. Syst.*, vol. 18, no. 5, pp. 1066–1077, May 2017.

[5] S. E. Li *et al.*, "Dynamical modeling and distributed control of connected and automated vehicles: Challenges and opportunities," *IEEE Intell. Transp. Syst. Mag.*, vol. 9, no. 3, pp. 46–58, Jul. 2017.

[6] S. E. Li, Y. Zhang, K. Li, L.-Y. Wang, and H. Zhang, "Platoon control of connected vehicles from a networked control perspective: Literature review, component modeling, and controller synthesis," *IEEE Trans. Veh. Technol.*, to be published.

[7] J. Jaguemont, L. Boulon, and Y. Dubé, "Characterization and modeling of a hybrid-electric-vehicle lithium-ion battery pack at low temperatures," *IEEE Trans. Veh. Technol.*, vol. 65, no. 1, pp. 1–14, Jan. 2016.

[8] R. Zhao, S. Zhang, J. Liu, and J. Gu, "A review of thermal performance improving methods of Lithium Ion battery: Electrode modification and thermal management system," *J. Power Sources*, vol. 299, pp. 557–577, Dec. 2015.

[9] G. Xia, L. Cao, and G. Bi, "A review on battery thermal management in electric vehicle application," *J. Power Sources*, vol. 367, pp. 90–105, Nov. 2017.

[10] D. Bernardi, E. Pawlikowski, and J. Newman, "A general energy balance for battery systems," *J. Electrochem. Soc.*, vol. 132, no. 1, pp. 5–12, 1985.

[11] A. A. Pesaran, "Battery thermal models for hybrid vehicle simulations," *J. Power Sources*, vol. 110, no. 2, pp. 377–382, 2002.

[12] K. Smith and C.-Y. Wang, "Power and thermal characterization of a lithium-ion battery pack for hybrid-electric vehicles," *J. Power Sources*, vol. 160, no. 1, pp. 662–673, 2006.

[13] X. Hu, S. Lin, S. Stanton, and W. Lian, "A foster network thermal model for HEV/EV battery modeling," *IEEE Trans. Ind. Appl.*, vol. 47, no. 4, pp. 1692–1699, Jul./Aug. 2011.

[14] Y. Hu, S. Yurkovich, Y. Guezennec, and B. J. Yurkovich, "Electro-thermal battery model identification for automotive applications," *J. Power Sources*, vol. 196, no. 1, pp. 449–457, 2011.

[15] K. Murashko, J. Pyrhönen, and L. Laurila, "Three-dimensional thermal model of a lithium ion battery for hybrid mobile working machines: Determination of the model parameters in a pouch cell," *IEEE Trans. Energy Convers.*, vol. 28, no. 2, pp. 335–343, Jun. 2013.

[16] J. Jaguemont, L. Boulon, P. Venet, Y. Dubé, and A. Sari, "Lithium-ion battery aging experiments at subzero temperatures and model development for capacity fade estimation," *IEEE Trans. Veh. Technol.*, vol. 65, no. 6, pp. 4328–4343, Jun. 2016.

[17] S. Bauer, A. Suchaneck, and F. P. León, "Thermal and energy battery management optimization in electric vehicles using Pontryagin's maximum principle," *J. Power Sources*, vol. 246, pp. 808–818, Jan. 2014.

[18] J. Jaguemont, L. Boulon, Y. Dubé, and F. Martel, "Thermal management of a hybrid electric vehicle in cold weather," *IEEE Trans. Energy Convers.*, vol. 31, no. 3, pp. 1110–1120, Sep. 2016.

[19] Q. Xie, D. Shin, N. Chang, and M. Pedram, "Joint charge and thermal management for batteries in portable systems with hybrid power sources," *IEEE Trans. Comput.-Aided Design Integr. Circuits Syst.*, vol. 35, no. 4, pp. 611–622, Aug. 2015.

[20] Y. Wang, Q. Gao, T. Zhang, G. Wang, Z. Jiang, and Y. Li, "Advances in integrated vehicle thermal management and numerical simulation," *Energies*, vol. 10, no. 10, pp. 1636–1666, Oct. 2017.

[21] T. Yuksel, S. Litster, V. Viswanathan, and J. J. Michalek, "Plug-in hybrid electric vehicle $LiFePO_4$ battery life implications of thermal management, driving conditions, and regional climate," *J. Power Sources*, vol. 338, pp. 49–64, Jan. 2017.

[22] X. Tao and J. Wagner, "A thermal management system for the battery pack of a hybrid electric vehicle: Modeling and control," *Proc. Inst. Mech. Eng., D, J. Automobile Eng.*, vol. 230, no. 2, pp. 1–12, Feb. 2016.

[23] J. Lopez-Sanz *et al.*, "Thermal management in plug-in hybrid electric vehicles: A real-time nonlinear model predictive control implementation," *IEEE Trans. Veh. Technol.*, vol. 66, no. 9, pp. 7751–7760, Sep. 2017.

[24] J. Lopez-Sanz *et al.*, "Nonlinear model predictive control for thermal management in plug-in hybrid electric vehicles," *IEEE Trans. Veh. Technol.*, vol. 66, no. 5, pp. 3632–3644, May 2017.

[25] Y. Masoudi and N. L. Azad, "MPC-based battery thermal management controller for Plug-in hybrid electric vehicles," in *Proc. Amer. Control Conf. (ACC)*, May 2017, pp. 4365–4370.

[26] F. Altaf, B. Egardt, and L. J. Mårdh, "Load management of modular battery using model predictive control: Thermal and state-of-charge balancing," *IEEE Trans. Control Syst. Technol.*, vol. 25, no. 1, pp. 47–62, Jan. 2017.

[27] C.-J. Chiang, J.-L. Yang, and W.-C. Cheng, "Temperature and state-of-charge estimation in ultracapacitors based on extended Kalman filter," *J. Power Sources*, vol. 234, pp. 234–243, Jul. 2013.

[28] L. Fan, J. M. Khodadadi, and A. A. Pesaran, "A parametric study on thermal management of an air-cooled Lithium-Ion battery module for plug-in hybrid electric vehicles," *J. Power Sources*, vol. 238, pp. 301–312, Sep. 2013.

[29] R. R. Richardson, P. T. Ireland, and D. A. Howey, "Battery internal temperature estimation by combined impedance and surface temperature measurement," *J. Power Sources*, vol. 265, pp. 254–261, Nov. 2014.

[30] R. R. Richardson and D. A. Howey, "Sensorless battery internal temperature estimation using a Kalman filter with impedance measurement," *IEEE Trans. Sustain. Energy*, vol. 6, no. 4, pp. 1190–1199, Oct. 2015.

[31] Y. Xiao, "Model-based virtual thermal sensors for lithium-ion battery in EV applications," *IEEE Trans. Ind. Electron.*, vol. 62, no. 5, pp. 3112–3122, May 2015.

[32] C. Zhang, K. Li, J. Deng, and S. Song, "Improved realtime state-of-charge estimation of $LiFePO_4$ battery based on a novel thermoelectric model," *IEEE Trans. Ind. Electron.*, vol. 64, no. 1, pp. 654–663, Jan. 2017.

[33] Q. Peng, H. Zhao, X. Liu, Y. Fang, and X. Zeng, "Battery thermal management system design and control strategy study for hybrid electric vehicles," in *Proc. IEEE Conf. Expo Transp. Electrific. Asia–Pacific (ITEC Asia-Pacific)*, Aug./Sep. 2014, pp. 1–4.

[34] M. J. Moran and H. N. Shapiro, *Fundamentals of Engineering Thermodynamics*, 5th ed. New York, NY, USA: Wiley, 2006.

[35] Z. Gao, "Active disturbance rejection control: A paradigm shift in feedback control system design," in *Proc. Amer. Control Conf.*, Jun. 2006, pp. 2399–2405.

[36] S. Li, J. Yang, W.-C. Chen, and X. Chen, "Generalized extended state observer based control for systems with mismatched uncertainties," *IEEE Trans. Ind. Electron.*, vol. 59, no. 12, pp. 4792–4802, Dec. 2012.

[37] T. Gray and M. Shirk, "2010 Toyota Prius VIN 0462 hybrid electric vehicle battery test results," Idaho Nat. Lab., Idaho Falls, ID, USA, Tech. Rep. INL/EXT-13-28025, Jan. 2013.

Chong Zhu (M'17) received the B.S. degree in electrical engineering from the China University of Mining and Technology, Xuzhou, China, in 2006, and the Ph. D. degree in electrical engineering from Zhejiang University, Hangzhou, China, in 2016.

He is currently a Post-Doctoral Researcher with San Diego State University, San Diego, CA, USA. His current research interests include battery thermal management, ac/dc power conversion, and pulse-width modulation techniques applied in EVs.

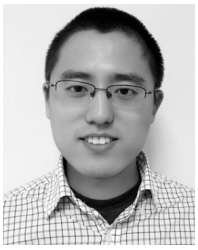

Fei Lu (S'12–M'17) received the B.S. and M.S. degrees in electrical engineering from the Harbin Institute of Technology, Harbin, China, in 2010 and 2012, respectively, and the Ph.D. in electrical engineering degree from the University of Michigan, Ann Arbor, MI, USA, in 2017.

He is currently a Post-Doctoral Researcher with San Diego State University, San Diego, CA, USA. His current research interests include the application of electric vehicle charging.

Hua Zhang (S'14–M'17) received the B.S., M.S., and Ph.D. degrees in electrical engineering from Northwestern Polytechnical University, Xi'an, China, in 2011, 2014, and 2017, respectively.

From 2014 to 2015, she was a Joint Ph.D. Student funded by the China Scholarship Council with the University of Michigan, Dearborn, MI, USA. Since 2015, she has been with San Diego State University, San Diego, CA, USA. Her current research interests include the charging technology of electric vehicles.

Chunting Chris Mi (S'00–A'01–M'01–SM'03–F'12) received the B.S.E.E. and M.S.E.E. degrees in electrical engineering from Northwestern Polytechnical University, Xi'an, China, in 1985 and 1988, respectively, and the Ph.D. degree in electrical engineering from the University of Toronto, Toronto, ON, Canada, in 2001.

From 2001 to 2015, he was with the University of Michigan, Dearborn, MI, USA. He is currently a Professor and the Chair of electrical and computer engineering and the Director of the Department of Energy-funded Graduate Automotive Technology Education Center for Electric Drive Transportation, San Diego State University, San Diego, CA, USA.